PERGAMON

Journal of Atmospheric and Solar-Terrestrial Physics 60 (1998) 863–870

Journal of ATMOSPHERIC AND SOLAR-TERRESTRIAL PHYSICS

Ionospheric effects due to electrostatic thundercloud fields

Victor P. Pasko,* Umran S. Inan, Timothy F. Bell

STAR Laboratory, Stanford University, Stanford, CA 94305, U.S.A.

Received 6 January 1997; accepted 11 February 1998

Abstract

Electrostatic thundercloud fields are shown to heat lower ionospheric electrons significantly under night time conditions. The effect is maximized under conditions of higher altitudes of thundercloud charges, larger magnitudes of these charges, and larger scale heights of ambient conductivity profiles. The lower ionospheric conductivity can be modified as a result of the heating by up to one order of magnitude in regions with a characteristic lateral extent of ~150 to 350 km. The vertical extent of the heated region is ~10 km, at altitudes of ~70–80 km, reaching above 85 km in some cases, depending on the ambient night-time conductivity profile. The electron heating may potentially alter the chemical balance in the D-region, modify the ambient levels of optical emissions and the magnitude of electrostatic thundercloud fields which map to higher ionospheric altitudes.

1. Introduction

The penetration of electrostatic (ES) thundercloud fields into the lower ionosphere was studied by a number of authors (see Tzur and Roble, 1985; Roble, 1991; Velinov and Tonev, 1995 and references cited therein). Recently experimental evidence has been put forth suggesting that ES fields are capable of maintaining the ionospheric electrons at a persistently heated level well above their ambient thermal energy (Inan et al., 1996). Changes in the thundercloud charge distributions (e.g. due to lighting discharges) lead to heating/cooling above/below this quiescent level, and the corresponding changes in the lower ionospheric conductivity are registered as early/fast perturbations of subionospherically traveling VLF signals (Inan et al., 1996). In the present paper, a two-dimensional electrostatic heating (ESH) model is developed to study the mapping of the ES fields to the ionosphere and the associated heating of the electron plasma. In contrast to previous work (e.g. Tzur and Roble, 1985; Velinov and Tonev, 1995) the model self-consistently accounts for the nonlinear dependence of the specific and Pedersen conductivities of the ionospheric plasma on the magnitude of the electric field (E) due to the electron heating. In comparison with (Inan et al., 1996) the ESH model is limited to calculations of the DC component of the electric field, includes the effects of the external geomagnetic field and extends the calculations to higher ionospheric altitudes. The ESH model does not consider lightning discharges, concentrating instead on integrated long term effects of quasi-static charge systems in thunderstorms and remains valid with very good accuracy as long as any lightning discharges which may occur remove only a small fraction of the total charge accumulated in a thunderstorm.

2. Model

The ESH model describes the electric field established in the conducting atmosphere, the mesosphere and the lower ionosphere due to static thundercloud charges $+Q$, $-Q$ which form a vertical dipole. A cylindrical coordinate system (r, ϕ, z) is used with the z axis representing altitude. The ground is assumed to be perfectly conducting and the entire system is assumed to be cylindrically symmetric about the z axis.

The electrostatic potential φ ($\vec{E} = -\nabla\varphi$) is calculated using the stationary continuity equation:

$$\nabla \cdot (\hat{\sigma}\nabla\varphi - \vec{J}_s) = 0 \tag{1}$$

where $\vec{J}_s$ is the density of the current maintaining the thundercloud charges against conduction loss and $\hat{\sigma}$ is the conductivity tensor of the medium. The conductivity

* Corresponding author. Tel.: 001 650 723 0338; fax: 001 650 723 9251; e-mail: PASKO@nova.stanford.edu

S0017–9310/98/$—See front matter
PII: S1364-6826(98)00022-4

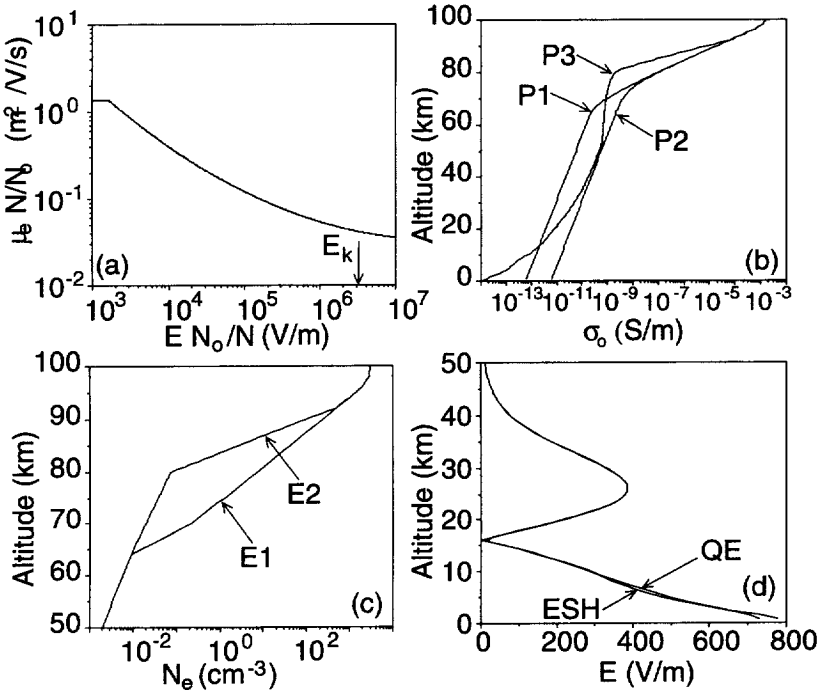

Fig. 1. (a) The electron mobility μ_e is shown as a function of the electric field and molecular number density of atmospheric gas N (Davies, 1983; Hegerberg and Reid, 1980; Pasko et al., 1997); (b) three models of ambient conductivity; (c) comparison of results of QE and ESH models.

can be expressed as the sum of scalar ion σ_i and tensor electron $\hat{\sigma}_e$ components: $\hat{\sigma} = \sigma_i + \hat{\sigma}_e$. The electron component is given as

$$\hat{\sigma}_e = \begin{pmatrix} \sigma_P & \sigma_H & 0 \\ -\sigma_H & \sigma_P & 0 \\ 0 & 0 & \sigma_o \end{pmatrix}$$

where σ_o, σ_P, and σ_H are the specific, Pedersen and Hall electron conductivities, respectively. Due to axial symmetry, the solution of (1) depends only on σ_o and σ_P which can be expressed as $\sigma_o = eN_e\mu_e$ and $\sigma_P = \sigma_o(1+\omega_H^2/\nu_{eff}^2)^{-1}$, where N_e is the electron number density, ω_H is the electron gyrofrequency, and $\nu_{eff} = e/(\mu_e m_e)$ is the effective electron collision frequency. The electron mobility μ_e is a strong function of the magnitude of the electric field due to the electron heating (Fig. 1a), which introduces nonlinearity into equation (1).

The current $\vec{J}_s$ in (1) can be expressed in the form $\nabla\vec{J}_s = -\rho_s\sigma_o/\varepsilon_o$, where ρ_s is the source charge density corresponding to the thundercloud charges. We assume that $\rho_s = \rho_+ + \rho_-$ represents each total dipole charge $\pm Q$ as a distributed charge density $\rho_\pm(r,t)$ with a Gaussian spatial distribution ($e^{-[(z-z_\pm)^2+r^2]/a^2}$) with $a = 3$ km, $z_- = 5$ km, $z_+ = 15$ km for negative and positive charges, respectively, and related to the total source charge as $\pm Q = \int \rho_\pm(r)\,dV$. The model also allows consideration of extended (in the horizontal direction) charge distributions similar to those which exist in mesoscale convective systems (MCS) (e.g. Marshall et al., 1996). In this case, the charge density is taken to have a Gaussian distribution ($e^{[(z-z_\pm)^2]/a^2}$) in the z direction and is assumed to be uniform in the r direction, with the scale defined as the radius of the 'disk' of charge.

The ESH model can treat different combinations of boundary conditions at the cylindrical (i.e. at $r = 200$ km) and at the upper ionospheric (i.e. at $z = 100$ km) boundaries: $\varphi = 0$, $\partial\varphi/\partial z = 0$, and $\partial\varphi/\partial r = 0$. We concentrate on heating effects in the altitude range 70–90 km. All of our results in this altitude range are found to be insensitive to the type of boundary conditions used in the calculations. We neglect fair weather E fields due to their relatively small amplitudes. The perfectly conducting ground ($z = 0$) is assumed to have zero potential ($\varphi = 0$).

We use three different ambient conductivity profiles as illustrated in Fig. 1b. Profile P1 consists of an ion conductivity distribution with altitude scale height 11 km, similar to that measured above thunderstorms (Holzworth et al., 1985) and the electron component calculated on the basis of the D-region electron density distribution used in previous work (e.g. Pasko et al., 1995; Inan et al., 1996) and marked E1 in Fig. 1c. The ion component of the conductivity is increased by a factor of

10 at each altitude for Profile P2. Profile P3 is a typical night time midlatitude profile taken from Hale (1994). The upper (lower ionospheric) part of this profile is defined by the electron distribution E2 shown in Fig. 1c.

Solution of the nonlinear equation (1) is obtained by simple iterations assuming its linearity during each iteration and starting with ambient conductivities (i.e. corresponding to $E = 0$). The linear problem is solved using Stone's strongly implicit procedure (Jesshope, 1979). In cases when convergence of Stone's method is not reached the solution is obtained using LAPACK (Anderson et al., 1995) sparse matrix methods which are more time consuming but always provide accurate solutions.

3. Results

We consider low intensity ES fields which can exist at high altitudes above thunderstorms during times between lightning discharges. No ionization effects are considered and the electric field is always assumed to be less than the threshold breakdown field (E_k) which is shown in Fig. 1a by an arrow (e.g. ~ 30 kV/cm at the sea level). The variation of μ_e implied by Fig. 1a is due to the electron heating in an applied DC field. It is important to note that heating is possible for a wide range of values of the electric field, extending to approximately three orders of magnitude below E_k.

Factors which control the penetration of ES fields to ionospheric altitudes can be understood qualitatively considering simplified analytical solutions obtained by Holzer and Saxon (1952) for the case of a monopole charge Q placed at altitude z_o above the Earth's surface in an atmosphere with exponentially increasing conductivity with scale height h, and ignoring the effects of image charges in the lower ionosphere. At distances $z \gg 2h$ and $z \gg z_o$, the electric field magnitude at $r = 0$ is simply $E \sim p(1 + z_o/2h)/(4\pi\varepsilon_o h^2 z)\, e^{-z/h}$, where $p = 2z_o Q$ is the dipole moment formed by charge Q and its ground image. From this simple consideration the effective penetration of thundercloud ES fields to ionospheric altitudes is maximized under conditions of: (1) higher altitudes of thundercloud charges; (2) larger magnitudes of these charges; (3) larger scale heights of ambient conductivity profiles. Factors (1) and (3) are directly connected with the number of atmospheric conductivity scale heights between the thundercloud source charge and the ionosphere. Most of the numerical results below can be qualitatively interpreted on the basis of these three factors.

Results are presented below for 7 different cases:

A1 thundercloud charges of $+100$ C and -100 C with $a = 3$ km at altitudes 15 and 5 km, respectively, with conductivity profile P1;
A2 same as A1 but with conductivity profile P2;
A3 same as A1 but with conductivity profile P3;
A4 thundercloud charges ± 1000 C at the same altitudes as in A1, with Gaussian distributions ($a = 3$ km) in the vertical dimension and disk-like distributions in the radial direction with radius 50 km, with conductivity profile P3;
A5 same as A4 but with conductivity profile P2;
A6 same as A3 but only with lower negative thundercloud charge, representative of conditions after the removal of the positive thundercloud charge by a positive cloud-to-ground (+CG) lightning discharge;
A7 same as A1 but assuming no heating effects of the electric field on conductivity.

3.1. Electric field

Figure 1d compares the results of calculations of the electric field using ESH and QE (Pasko et al., 1995) models for the static charge $+10$ C with $a = 10$ km at 20 km altitude. The QE model was run for 200 s, comparable to the local relaxation time at the ground level as required for the establishment of a time-stationary solution. The agreement between the two models is very good as expected from simple physical arguments. The important advantages of the ESH model are that it allows relatively fast solutions for static cases and significantly extends the upper boundary of the regions which can be modeled (Inan et al., 1996).

Figure 2a shows the distribution of the electric field for the cases A1–A4, A6 and A7. The electric field begins to decay dramatically starting at the altitude at which the electron component of the conductivity (typically with scale heights 1–3 km) dominates above the ion conductivity (which has scales ~ 11 km). In case A2, the ion conductivity is a factor of 10 greater than for case A1, leading to better penetration of the electric field to higher altitudes. For cases A3 and A4, the electron conductivity has a very sharp scale (~ 1.4 km scale height); however, it becomes important only above ~ 80 km where we see a significant reduction of the electric field with altitude. For case A4, the electric field is the largest preliminary due to the large source charge value of 1000 C.

3.2. Collision frequency

Figure 2b shows the distribution of ν_{eff} as a function of altitude for cases A1–A5. The electric fields described in the previous subsection lead to a modification (by more than one order of magnitude) of the lower ionospheric ν_{eff} which may extend in altitude up to 87 km (for the case A4). Results marked A6 in Figs. 2a and b illustrate the concept of the change in the level of E fields in the lower ionosphere and resulting cooling and decrease in ν_{eff} registered as early/fast VLF events (Inan et al., 1996) following removal of the thundercloud charge by a +CG discharge (in the case shown). Case A1 in Fig. 2b agrees

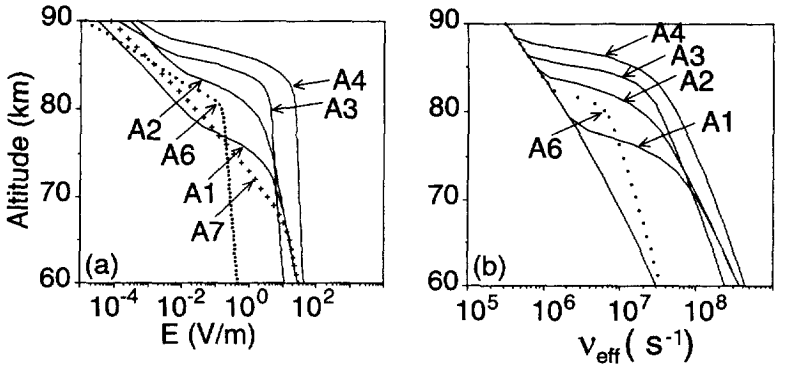

Fig. 2. Altitude scans at $r = 0$ of the electric field (a) and ν_{eff} (b), corresponding to different cases as described in the text.

with the altitude extent of the heated region obtained by Inan et al. (1996) for the same ambient conditions (e.g. electron and ion conductivity profiles).

3.3. Conductivity

Figure 3 shows the results of calculations of the modifications of σ_o and σ_P for cases A1–A4. Due to the electron heating and the increase in ν_{eff} ($\nu_{eff} \gg \omega_H$), both σ_o and σ_P tend to coincide at low altitudes. This result demonstrates that, in cases of intense electron heating, neglecting the effects of the geomagnetic field is a reasonable assumption (Pasko et al., 1995; Inan et al., 1996). The characteristic lateral extent of the lower ionospheric regions within which the conductivity is modified by heating (e.g. up to one order of magnitude as in case A4 at altitude ~85 km) varies from ~150–200 km in cases A1 and A2 to ~250–350 km in cases A3 and A4. The specific component of the conductivity in the disturbed regions (which controls the penetration of the vertical component of the electric field) tends to decrease at lower altitudes due to electron heating but then sharply increases reaching ambient values at higher altitudes. The decrease tends to smooth out the vertical gradient of the conductivity and leads to better penetration of the electric field. However, at higher altitudes where the gradient of the conductivity is significantly sharpened, the electric field is selfconsistently reduced. The net effect is that electric field amplitudes in ionospheric regions near ~90 km are ~70% lower, as a result of heating, as can be seen from a comparison of results A1 and A7 in Fig. 2a.

4. Discussion

4.1. Comparison with observations

The distribution of the electric field at thundercloud altitudes for different cases is shown in Fig. 4a and agrees well with reported magnitudes of E fields up to 100 kV/m measured in regions of thunderstorms (e.g. Winn et al., 1974; Marshall et al., 1996). We note that the electric field corresponding to case A4 (which leads to the largest heating effects at ionospheric altitudes) produces the smallest E fields inside the thundercloud (few kV/m). the effective surface charge density corresponding to 1000 C spread over a disk with radius 50 km is ~130 nC/m^2 which is several times lower than the values of 400–1200 nC/m^2 suggested by Marshall et al. (1996), indicating that the thundercloud charge magnitudes used in our calculations are rather conservative.

4.2. Heating of the neutral atmosphere

The ES fields may persist in the lower ionosphere for several hours leading to the heating of the atmosphere through collisional transfer of energy from electrons to neutrals. An upper bound estimate can be made by ignoring any losses. Assuming the heated electron temperature to be ~1 eV, the change in the temperature of the neutrals T can be estimated from the equation $dT/dt \sim \delta \nu_{eff} T_e N_e / N$, where $\delta \sim 5 \times 10^{-3}$ is the average fraction of energy transferred in one collision from electrons to neutrals (Gurevich, 1978, p. 86). At 85 km altitude, this leads to a heating rate of $dT/dt \sim 10^{-3}$°K/s, indicating that ~10°K variation in the neutral temperature may occur over a time scale of 2–3 h. This estimated heating rate may compete with integral daily heating produced by solar radiation (see discussion in Hines, 1965) and is of the same order of magnitude as was measured in the mesosphere above thunderstorms and interpreted as heating by internal gravity waves generated by tropospheric convection (e.g. Taylor, 1979). The integrated effect of both types of heating might be important since only 10% variation in the atmospheric neutral density would lead to ~100% variation in the effective ionization rate (e.g. Papadopoulos et al., 1993) and may in turn significantly modify the structure of ionization regions associated with sprites following inten-

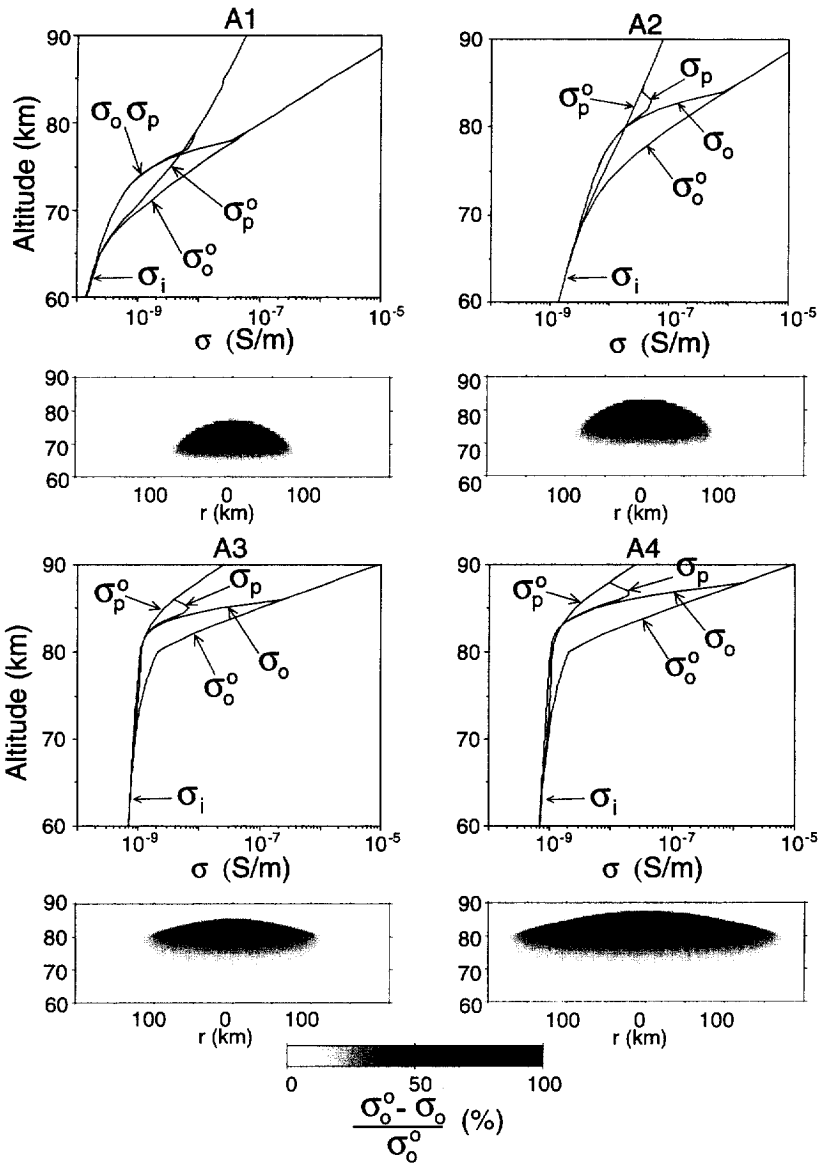

Fig. 3. *Lower panels* show a cross sectional view of the distribution of the relative change (%) in specific conductivity corresponding to cases A1–A4. *Upper panels* show altitude scans at $r = 0$ of ambient (marked by o upper index) and modified (by heating) specific and Pedersen conductivities for cases A1–A4.

sive positive lightning discharges (e.g. Pasko et al., 1997, and references therein).

4.3. Chemical balance of the D-region

The heating of electrons by ES fields may lead to significant modification of the chemical balance of the lower ionosphere (e.g. Rodriguez and Inan, 1994). Simple analytical estimates of this effect can be obtained by assuming that the electron attachment, detachment and dissociative recombination with cluster ions are the dominant processes controling the electron balance in the lower ionosphere (see Rodriguez and Inan, 1994, and references cited therein). In the stationary case, and assuming that the electron attachment dominates over the detachment and has the functional dependence on

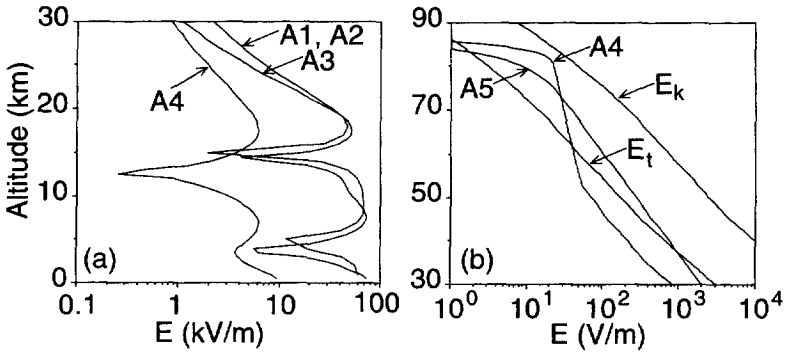

Fig. 4. Altitude scans at $r = 0$ of the module of the electric field in a region of a thundercloud for cases A1–A4 (a), and in the altitude range 30–90 km for cases A4 and A5 (b). The left panel also has altitude distributions of conventional (E_k) and runaway (E_t) threshold breakdown fields. The electric field is positive (directed upward) for altitudes $z > \sim 15$ km and $z < \sim 5$ km and negative for altitudes $5 < z < 15$ km, thus changing sign at altitudes ~ 5 and ~ 15 km.

the electron temperature T_e given by Tomko et al. (1980), the relative change in the electron number density can be expressed as

$$\frac{N_e(T_e)}{N_{eo}} = \sqrt{\frac{T_e}{T} e^{\frac{700}{T_e} - \frac{700}{T}}},$$

where N_{eo} is the unperturbed electron density and T is the temperature of the neutrals. The electron density reaches a minimum value of $N_e \sim 0.58 N_{eo}$ at $T_e = 700$ K, returns to ambient level $N_e \sim N_{eo}$ at $T_e = 6000$ K and reaches the value $N_e \sim 1.26 N_{eo}$ at $T_e = 10^4$ K. Thus, the value of N_e can vary by a factor of 2 over this temperature range.

The detachment of electrons from oxygen molecules in collisions with molecular oxygen (with rate $\sim e^{-5590/T}$ (e.g. Kozlov et al., 1987)) may be important in cases of significant heating of the neutral atmosphere above thunderstorms. For example, a 5% increase in T from 200 to 210°K estimated in the previous section would lead to a factor of ~ 4 increase in the detachment coefficient. Under certain conditions detachment may exceed attachment and lead to an increase in N_e.

4.4. Excitation of optical and infrared emissions

As can be seen from Fig. 4b, the electric field for case A4 at altitude 83 km is only two times less than E_k. Estimates indicate that the electron distribution function for such fields already has a significant fraction of electrons in energy regions of vibrational excitation of N_2 molecules (~ 2 eV) as well as excitation of first positive band of N_2 (~ 7 eV). Assuming the lateral extent of the excited region to be ~ 100 km, using the optical emission excitation rates as a function of the electric field as given in Pasko et al. (1997) and integrating along a horizontal line of sight gives $\sim 10^2$ kR for the first positive and 1 kR for the second positive bands of N_2. This intensity of the first positive band is comparable to ambient levels; however, the altitude extent of the optical emission would be very narrow (~ 1 km).

Estimations of production rates of vibrationally excited N_2 molecules lead to estimates of $\sim 10^6$ cm^{-3} s^{-1} at altitudes ~ 85 km, which is well above ambient levels (e.g. Kumer et al., 1978) and which may lead to significant enhancements of infrared radiation in the lower ionosphere (Picard et al., 1997).

4.5. Runaway electrons

Figure 4b shows the distribution of the electric field corresponding to cases A4 and A5 as well as threshold fields for conventional E_k (Papadopoulos et al., 1993) and runaway E_t (e.g. Bell et al., 1995) breakdown as functions of altitude. The upward runaway process may be possible between lightning discharges only in cases when the negative charge is at the thundercloud top and the positive at the bottom. The heating effects and amplitudes of calculated E fields described above do not depend on the polarity of the charges. Thus, we can use the same E fields for different polarities of charges. For case A4, the runaway process starts at an altitude ~ 68 km above which $\delta_o = E/E_t > 1.5$ (Bell et al., 1995), and for case A5 at an altitude ~ 50 km. The production rate of runaway electrons can be estimated as $S_o = 2.5 \times 10^{-8}$ cm^{-3} s^{-1} at 50 km and $S_o = 3 \times 10^{-9}$ cm^{-3} s^{-1} at 68 km altitude (Bell et al., 1995). For case A4, δ_o increases with altitude and equals ~ 2 at 70 km, ~ 3 at 75 km, ~ 7 at 80 km and ~ 10 at 85 km. For a first order estimate, we can assume that $\delta_o \sim 5$ over the entire range of altitudes between 68 and 85 km. For case A5, $\delta_o \sim 2$ is a good approximation in the altitude range 50–75 km. Runaway e-folding distances are $l = 5.8$ km at 50 km altitude for case A5 and $l = 13.1$ km at 68 km for case A4. Resulting runaway number densities escaping to the magnetosphere

are estimated as $N_R \sim 10^{-10}$ cm^{-3} for case A5 and $N_R \sim 10^{-13}$ cm^{-3} for case A4. These estimates show that the number densities are too small to produce any significant effects such as the heating of neutrals or excitation of observable optical emissions. The upward going energy flux is estimated for case A5 to be 5×10^{-6} erg cm^{-2} s^{-1}. Since runaway electrons can be launched to the magnetosphere continuously over a time scale of several hours, their integral effects as a source of the high energy ($\sim$1–10 MeV) population of the radiation belts and continuous production of ionization at low atmospheric altitudes (including effects in the conjugate hemisphere) might be important and need to be evaluated.

4.6. *Ionospheric modifications before earthquakes*

It has been proposed that quasistatic E fields $\sim$10 kV/m at sea level can be generated before earthquakes (e.g. Gokhberg et al., 1984). These fields are comparable to those of thunderclouds and thus may be expected to produce similar heating effects in the lower ionosphere. It is illustrative to estimate the scale of atmospheric conductivity for which a 10 kV/m E field at sea level can penetrate to the ionosphere and produce electron heating. At 80 km altitude the magnitude of the conventional breakdown field is $\sim$50 V/m (see Fig. 4b, for example), so that, following our previous discussion, to produce heating effects the electric field should be at least 10^{-3} $E_k \sim 50$ mV/m at this altitude. Simple calculations give a minimum required scale of atmospheric conductivity of 6.55 km, which is well in the range of values generally accepted in literature (e.g. Velinov and Tonev, 1995).

5. Summary

A two-dimensional cylindrically symmetric electrostatic heating (ESH) model is developed to study the mapping of the thundercloud electric fields to the ionosphere and the associated heating of the electron plasma. The model selfconsistently accounts for the nonlinear dependence (due to the electron heating) of the specific and Pedersen conductivities of the ionospheric plasma on the magnitude of the electric field. Application of the model under a variety of night-time atmospheric and thunderstorm conditions allows a detailed quantitative assessment of the geometry and physical characteristics of the modified lower ionospheric regions. The heating effect is maximized under conditions of higher altitudes of thundercloud charges, larger magnitudes of these charges, and larger scale heights of the ambient conductivity profiles. The lower ionospheric conductivity can be modified as a result of the heating by up to one order of magnitude in regions with characteristic lateral extent of $\sim$150–350 km. The vertical extent of the heated region is $\sim$10 km, at altitudes of $\sim$70–80 km, reaching above 85 km in some cases, depending on the ambient conductivity profile. The electron heating may potentially alter the chemical balance in the D-region, modify the ambient levels of optical emissions and the magnitude of electrostatic thundercloud fields which map to higher ionospheric altitudes.

Acknowledgements

This work was sponsored by the NSF grant ATM-9522816 and NASA grant NAGW-5-6264 to Stanford University.

References

Anderson, E., et al., 1995. LAPACK Users' Guide, second edn, SIAM.

Bell, T.F., Pasko, V.P., Inan, U.S., 1995. Runaway electrons as a source of red sprites in the mesosphere. Geophys. Res. Lett. 22, 2127.

Davies, D.K., 1983. Measurements of swarm parameters in dry air. Theoretical Notes, Note 346, Westinghouse R&D Center, Pittsburg, May.

Gokhberg, M.B., et al., 1984. Possible effects of the action of electric fields of seismic origin on the ionosphere. Geomag. Aeron. 24, 183.

Gurevich, A.F., 1978. Nonlinear phenomena in the ionosphere, Springer-Verlag, Berlin.

Hale, L.C., 1994. Coupling of ELF/ULF energy from lightning and MeV particles to the middle atmosphere, ionosphere, and global circuit. J. Geophys. Res. 21089.

Hegerberg, R., Reid, I.D., 1980. Electron drift velocities in air, Aust. J. Phys. 33, 227.

Hines, C.O., 1965. Dynamical heating of the upper atmosphere. J. Geophys. Res. 70, 177.

Holzer, R.E., Saxon, D.S., 1952. Distribution of electrical conduction currents in the vicinity of thunderstorms. J. Geophys. Res. 57, 207.

Holzworth, R.H., Kelley, M.C., Siefring, C.L., Hale, L.C., Mitchell, J. T., 1985. Electrical measurements in the atmosphere and the ionosphere over an active thunderstorm. 2. Direct current electric fields and conductivity. J. Geophys. Res. 90, 9824.

Inan, U.S., Pasko, V. P., Bell, T.F., 1996. Sustained heating of the ionosphere above thunderclouds as evidenced in "early/fast" VLF events. Geophys. Res. Lett. 23, 1067.

Jesshope, C.R., 1979. SIPSOL—a suite of subprograms for the solution of the nonlinear equations arising from elliptic partial differential equations. Computer Phys. Comm. 17, 383.

Kozlov, S.I., Vlaskov, V.A., Smirnova, N.V., 1988. Specialized aeronomic model for investigating artificial modification of the middle atmosphere and lower ionosphere, 1, Requirements of the model and basic concepts of its formation. Cosmic Res. 26, 635.

Kumer, J.B., Stair, A.T., Wheeler, Ned, Baker, K.D., Baker, D.J., 1978. Evidence for an OH* $\rightarrow N_2^* \rightarrow CO_2(v_3) \rightarrow CO_2 + h\nu$ (4.3 μm). J. Geophys. Res. 83, 4743.

Marshall, T.C., Stolzenburg, M., Rust, W.D., 1996. Electric field measurements above mesoscale convective systems. J. Geophys. Res. 101, 6979.

Papadopoulos, K., Milikh, G., Gurevich, A., Drobot, A., Shanny, R., 1993. Ionization rates for atmospheric and ionospheric breakdown. J. Geophys. Res. 98, 17593.

Pasko, V.P., Inan, U.S., Taranenko, Y.N., Bell, T.F., 1995. Heating, ionization and upward discharges in the mesosphere due to intense quasi-electrostatic thundercloud fields. Geophys. Res. Lett. 22, 365.

Pasko, V.P., Inan, U.S., Bell, T.F., Taranenko, Y.N., 1997. Sprites produced by quasi-electrostatic heating and ionization in the lower ionosphere. J. Geophys. Res. 102, 4529.

Picard, R.H., Inan, U.S., Pasko, V.P., Winick, J.R., Wintersteiner, P.P., 1997. Infrared glow above thunderstorms? Geophys. Res. Lett. 24, 2635.

Roble, R.G., 1991. On modeling component processes in the Earth's global electric circuit. J. Atmos. Terr. Phys. 53, 831.

Rodriguez, J.V., Inan, U.S., 1994. Electron density changes in the nighttime *D* region due to heating by very-low-frequency transmitters. Geophys. Res. Lett. 21, 93.

Tomko, A.A., Ferraro, A.J., Lee, H.S., Mitra, A.P., 1980. A theoretical model of D-region ion chemistry modifications during high power radio wave heating. J. Atmos. Terr. Phys. 42, 275.

Taylor, L.L., 1979. Mesospheric heating due to intense tropospheric convection. NASA Contractor Report 3132, Washington, D.C.

Tzur, I., Roble, R.G., 1985. The interaction of a polar thunderstorm with its global electrical environment. J. Geophys. Res. 90, 5989.

Velinov, P.I., Tonev, P.T., 1995. Modeling the penetration of thundercloud electric fields into the ionosphere. J. Atmos. Terr. Phys. 57, 687.

Winn, W.P., Schwede, Moore, C.B., 1974. Measurements of electric field in thunderclouds. J. Geophys. Res. 79, 1761.